



Synthesis of Bi₂S₃ microsphere and its efficient photocatalytic activity under visible-light irradiation

Guo-qing ZHAO^{1,2}, Yi-jian ZHENG¹, Zhi-guo HE³, Ze-xiang LU⁴,
Long WANG¹, Cai-feng LI¹, Fei-peng JIAO^{1,2}, Chun-yan DENG¹

1. School of Chemistry and Chemical Engineering, Central South University, Changsha 410083, China;
2. Hunan Provincial Key Laboratory of Efficient and Clean Utilization of Manganese Resources, Central South University, Changsha 410083, China;
3. School of Minerals Processing and Bioengineering, Central South University, Changsha 410083, China;
4. Department of Chemical Engineering, College of Materials Engineering, Fujian Agriculture and Forestry University, Fuzhou 350002, China

Received 15 July 2017; accepted 26 February 2018

Abstract: A novel Bi₂S₃ microsphere was fabricated through one-pot urea-assisted solvothermal method. The synthesized Bi₂S₃ microsphere was characterized by X-ray diffraction (XRD), scanning electron microscopy (SEM), Fourier transformed infrared spectroscopy (FT-IR) and thermal gravimetric analysis and differential thermal analysis (DTA-TG). Subsequently, the photocatalytic performances of Bi₂S₃ microsphere were evaluated by photocatalytic degradation of methyl orange (MO) simulation solution under visible-light irradiation. The results show that, Bi₂S₃ microsphere could be used as a potential cost-efficient catalysis for eliminating of methyl orange from aqueous solutions, whose degradation rate could reach 91.07% within 180 min. Besides, a tentative photocatalytic reaction mechanism was discussed according to the energy band position. Therefore, this work indicated a simplistic approach for the fabrication of visible-light responsive Bi₂S₃ microsphere photocatalyst, which can be used as a valuable candidate in solar energy conversion and environment pollution treatment.

Key words: Bi₂S₃ microsphere; hydrothermal methods; photocatalytic degradation

1 Introduction

With the development of social economy and living standards improving, a variety of dyes are synthesized to meet the demands of mankind. However, a great deal of synthetic dyes are observed in the effluent of many industries, which contain fibrous materials, stock, chemicals, surfactant, leather, plastic, dye manufacturing and finishing agent [1–3]. As we all know, many dyes are potentially hazardous and the discharge of toxic materials into water can often cause serious harms to aquatic organisms. Therefore, how to remove them from industrial effluents has been become a major environmental issue in recent years [4,5]. Meanwhile, the conventional waste-water treatment methods have been

used to remove dye-contaminated waste water, such as adsorption, chemical oxidation, reverse osmosis, extraction and photocatalytic degradation [6–8]. Among these methods, photocatalytic degradation is considered to be one of the preferred route because of its high efficient, simplicity, remarkable ability and low cost [9].

Recently, semiconductor photocatalytic degradation of organic pollutants has received much attention because of its remarkable ability to decompose organic pollutants into harmless substances immediately from the contaminant source in the UV exposure. Bi₂S₃ is one of excellence semiconductor and it has drawn broad attention on Schottky diode [10], solar cells [11], sensors [12], supercapacitor electrodes [13] and thermoelectric devices [14]. Besides, Bi₂S₃ particles have narrow band gap ($E_g=1.3$ eV) and high absorption

Foundation item: Projects (21476269, 21776319) supported by the National Natural Science Foundation of China; Project (2016TP1007) supported by Hunan Provincial Science and Technology Plan Project of China; Project (2017J01569) supported by the Natural Science Foundation of Fujian Province, China; Project (201710533255) supported by National College Students' Free Exploration Project of China; Project (2017zzts777) supported by Fundamental Research Funds for the Central Universities of Central South University, China

Corresponding author: Fei-peng JIAO, Tel: +86-731-88830833, E-mail: jiaofp@163.com; Chun-yan DENG, E-mail: dengchunyan@csu.edu.cn
DOI: 10.1016/S1003-6326(18)64844-7

coefficient for photocatalysis. So, by comparison, it shows extensive application market in the photocatalysis [15–18]. Thanks to the remarkable photocatalytic performance of Bi_2S_3 particles, the Bi_2S_3 products have been used as photocatalyst to solve waste water polluted by dyes, such as Congo red (CR), methyl orange (MO), and acid yellow.

HU et al [19] hydrothermally synthesized different morphologies Bi_2S_3 nanostructures, such as nanorods, nanotubes, and nanowires, using ethanol as a surfactant. The prepared Bi_2S_3 nanostructures improved photocatalytic degradation of Cr(VI) under visible light irradiation. PRABHAKAR VATTIKUTI et al [20] synthesized Bi_2S_3 nanorods by a simple hydrothermal method using sodium sulfide as sulfur sources and H_2O_2 as frame developing agent. However, highly crystalline Bi_2S_3 nanorods needed higher roasting temperature. These results indicate that different surfactants introduced demonstrate a superior photocatalytic performance, which can be because of their higher crystalline, large specific surface area and more catalytic activity sites, etc. All in all, many problems limit their commercial application. Many efforts must be paid to further improve Bi_2S_3 photocatalysis under visible light illumination. Thus, in order to change the Bi_2S_3 photocatalysts status, the design and preparation of novel structures have become hot topics for improving organic pollutant degradation efficiency.

Herein, the Bi_2S_3 microsphere photocatalyst was prepared via a simple one-pot hydrothermal method at the fixed reaction parameters. The as-prepared samples were characterized by XRD, SEM, FT-IR, DTA-TG and their photocatalytic properties were studied by MO stimulation wastewater. Furthermore, the photocatalysis kinetics and a possible mechanism for the MO dyes degradation over Bi_2S_3 microsphere were proposed.

2 Experimental

2.1 Chemicals and materials

All chemicals were of analytic grade and used without being further purified. Bismuth nitrate ($\text{Bi}(\text{NO}_3)_3 \cdot 5\text{H}_2\text{O}$) (mass fraction 0.990) was provided by Xilong Chemical Co., Ltd., Beijing, China. Thiourea ($\text{CH}_4\text{N}_2\text{S}$) (mass fraction 0.990) was purchased from Damao Chemical Reagent Factory, Tianjin, China. Urea ($\text{CH}_4\text{N}_2\text{O}$) (mass fraction 0.990) was supplied by Evergreen Chemical Manufacturing Co., Ltd., Tianjin, China. Methyl orange (MO, $\text{C}_{14}\text{H}_{14}\text{N}_3\text{SO}_3\text{Na}$, mass fraction 0.990) was provided by Hengxing Chemical Manufacturing Co., Ltd., Tianjin, China. The mass fractions of these reagents were analyzed by high performance liquid chromatography (HPLC, Agilent 1260, America). The deionized water was used for

preparing the sample solutions. The details of chemicals used in this study are presented in Table 1.

Table 1 Source and properties of selected chemicals in experiment

Chemical	Relative molecular mass	Source	Purity	Method for purity determination
Bismuth nitrate	485.07	Xilong Chemical Co., Ltd., Beijing, China	0.990	HPLC
Thiourea	76.12	Damao Chemical Reagent Factory, Tianjin, China	0.990	HPLC
Urea	60.06	Evergreen Chemical Manufacturing Co., Ltd., Tianjin, China	0.990	HPLC
Methyl orange	327.34	Hengxing Chemical Manufacturing Co., Ltd., Tianjin, China	0.990	HPLC

2.2 Synthesis of Bi_2S_3 microsphere

Bi_2S_3 microsphere was prepared by the one-pot hydrothermal method in this work [21–23]. Typically, this method adopted two solutions: A and B. Solution A including 4 mmol of thiourea in 20 mL of deionized water, was dropwise cautiously added to a violently stirred solution B, containing 4 mmol of $\text{Bi}(\text{NO}_3)_3 \cdot 5\text{H}_2\text{O}$ and 1.0 mol/L urea in 40 mL deionized water. Then, the mixed solvents were vigorously stirred continually for 30 min. Subsequently, the mixed solution was transferred into a Teflon-lined stainless steel autoclave and placed in ovens at 120 °C for 12 h. Finally, the obtained specimens were accumulated by centrifugation, washed with anhydrous ethanol and distilled water more than six times, and dried at 60 °C overnight. The detail schematic representation for preparation of Bi_2S_3 microsphere is show in Fig. 1.

2.3 Characterization of photocatalysts

The crystallinity and phase analyses of the synthesized Bi_2S_3 microspheres were investigated by using a powder X-ray diffractometer (Bruker D8) under the following condition: Cu K_α radiation, $\lambda=1.5406 \text{ \AA}$, 40 kV, 40 mA, and the data were obtained at a scanning rate of 8 (°)/min from $2\theta=5^\circ$ to $2\theta=80^\circ$. The morphology and size of the catalysts were observed by scanning

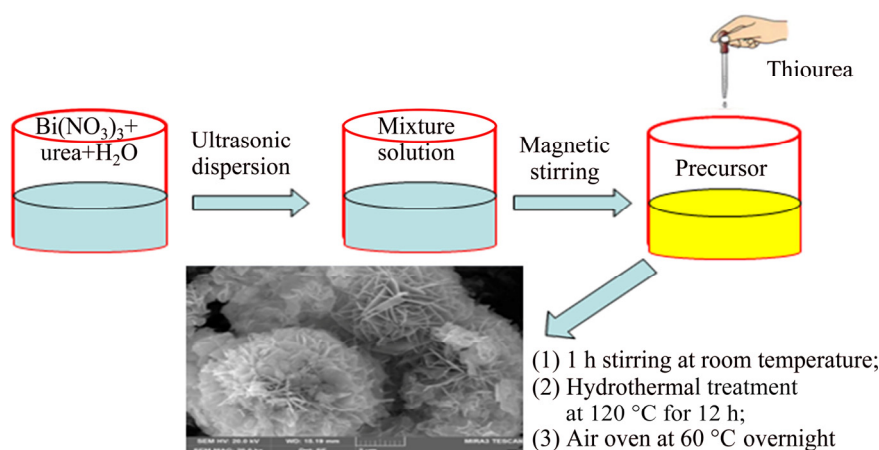


Fig. 1 Schematic representation for preparation of Bi_2S_3 microspheres

electron microscopy (SEM), which was provided by TESCAN MIRA3 LMU microscope. In situ FT-IR spectra were recorded by using an AVATAR 360 spectrometer in the range of $4000\text{--}400\text{ cm}^{-1}$. The thermal gravimetric analysis and differential thermal analysis (DTA-TG) was taken from room temperature to $950\text{ }^\circ\text{C}$ under an argon atmosphere on the instrument with the temperature increasing linearly at a rate of $10\text{ }^\circ\text{C}/\text{min}$, which was tested by SDT Q 600 simultaneous DSC-TGA instrument.

2.4 Photocatalytic activity testing

The photocatalytic performances of the Bi_2S_3 microsphere were evaluated by the discoloration of MO dyes solution under visible light irradiation. In a typical work, the reaction system including 50 mg Bi_2S_3 microsphere and aimed decomposed produce 50 mL MO (aqueous solution, 25 mg/L) was placed in the dark, which was maintained vigorously stirring to reach the adsorption/desorption equilibrium. Then, it was located under the light irradiation from a 500 W high pressure mercury lamp using the photochemical reaction apparatus (YM-GHX-V), which was provided by Yuming Instrument Co., Ltd., Shanghai, China. 3 mL of the reaction suspension solvent was taken every 20 min by a syringe with an attached filter (PTFE: $0.22\text{ }\mu\text{m}$). Subsequently, the concentration of MO was determined using a UV-vis spectrophotometer (UV-9600) at a set of wavelength. Considering the possible self-degradation of MO, the blank sample was seated under the same conditions without adding any Bi_2S_3 microsphere. The photocatalytic efficiency of MO degradation was calculated by using the following formula [24]:

$$P = [(C_0 - C) / C_0] \times 100\% \quad (1)$$

where P stands for the photocatalytic efficiency; C_0

represents initial MO concentration at $t=0$; and C is the MO concentration in the solvents at reaction time t .

3 Results and discussion

3.1 Characterization of samples

3.1.1 XRD

Figure 2 represents the XRD patterns of the synthesized Bi_2S_3 microsphere with different concentrations of mineralizer. As found in Fig. 2, with the concentration of mineralizer increasing, the impurity peaks of the sample are decreased. It is obviously found that the diffraction peaks of samples become purity when the concentration of mineralizer increases to 1.0 mol/L. Besides, the diffraction peaks of Bi_2S_3 microsphere are fundamental corresponding to the orthorhombic phase Bi_2S_3 (JCPDS: 17-0320, $a=1.114\text{ nm}$, $b=1.130\text{ nm}$, $c=0.398\text{ nm}$) [25]. The experimental result shows that the mineralizer and excessive sulfur ion are beneficial to

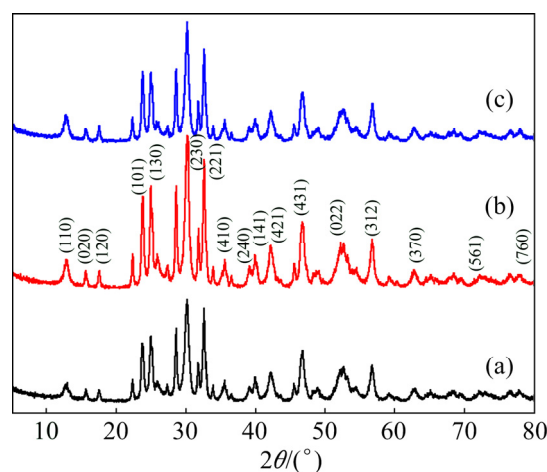


Fig. 2 XRD patterns of Bi_2S_3 microspheres photocatalysts with different concentrations of mineralizer: (a) 0.8 mol/L; (b) 1.0 mol/L; (c) 1.2 mol/L

form pure Bi_2S_3 microsphere. In addition, the sharp peaks of products illustrate that the hydrothermal reaction conditions are conducive to form good crystallization performance.

3.1.2 SEM

The morphological and microstructural particulars of the as-prepared samples were examined by the scanning electron microscopy (SEM). The SEM images of Bi_2S_3 microsphere at different hydrothermal synthesis temperatures are shown in Fig. 3. It is clearly found that the flowers-like Bi_2S_3 microspheres were synthesized at the reaction temperature of 120 °C. The hierarchical Bi_2S_3 microspheres render out a uniform size and good dispersion in morphology, which is composed of large amounts of thin sheets structure. However, from Fig. 3(b), it can be found that Bi_2S_3 has obvious rod-structure at 140 °C. Furthermore, the Bi_2S_3 rods present uneven distribution, which may be due to the flowers-like microspheres disturbed. Figure 3(c) displays the SEM image of Bi_2S_3 microspheres, which intuitively confirmed that the morphology of products is film with flower-like structure equally. However, Fig. 3(c) shows that the prepared samples are not uniform and have different sizes. Thus, with the reaction temperature increasing, the morphologies of Bi_2S_3 microsphere or material sizes were different. In generally, Bi_2S_3 microsphere tends to form flower shape, sheet, or rods at different reaction temperatures. In our study, the Bi_2S_3 flower-like microspheres were formed by the hydrolysis of $\text{Bi}(\text{NO}_3)_3$ and reaction with thiourea. Besides, the urea solution environment is helpful to form the flowers-like structure of the Bi_2S_3 microspheres.

3.1.3 FT-IR

Figure 4 illustrates the FT-IR spectra of obtained Bi_2S_3 microsphere, which shows demonstrative variation in the shape and position of signal peaks. It can be obviously discovered that the interaction occurred between excessive S^{2+} and Bi_2S_3 microsphere in the

process of synthesis, which can make the peaks shift slightly. As demonstrated in Fig. 4, the peak at 3400 cm^{-1} was attributed to the O—H stretching vibration, which corresponds to the internal water molecules of the prepared samples. The strong bands at approximately 2400 , 1630 and 1300 cm^{-1} arose from the C=O stretching vibration, N—H stretching vibration, and C—N stretching vibration of the urea mineralizer, respectively, which can be conjectured that the urea mineralizer has effects on the Bi_2S_3 photocatalysts [26]. The two peaks at 1100 and 842 cm^{-1} are ascribed to Bi—S bonds. However, the two diffraction peaks at 1100 and 842 cm^{-1} are due to the interaction between urea solution and Bi_2S_3 photocatalysts [27]. Combining the results of XRD and SEM, the flowers-like Bi_2S_3 microspheres were successfully constructed by a simple route.

3.1.4 TG-DTA

The thermal stability of the Bi_2S_3 microspheres was studied by the thermal gravimetric analysis (TG) and differential thermal analysis (DTA), which was tested under argon atmosphere from room temperature to 950 °C at heating rate of 10 °C/min, as shown in Fig. 5. The TG plots of samples showed a three-step decomposition pattern. The mass loss appeared below 100 °C was due to the evaporation of external surface and internal pores water, which has a corresponding broad weak exothermic peak in the DTA curve, as same as the above analysis of the FT-IR (Fig. 4) [28]. At the temperature higher than 100 °C, the mass loss of 8.91% for the samples corresponds to the loss of urea molecule and sulfur atom. At the third composition step at 465.46 °C, the mass loss of 32.06%, was attributed to the decomposition of Bi_2S_3 microspheres at the higher temperature. Besides, Fig. 5 shows strong exothermic peak at 465.46 °C in the DTA curve, which may be due to the decomposition of Bi_2S_3 microsphere at this temperature [29].

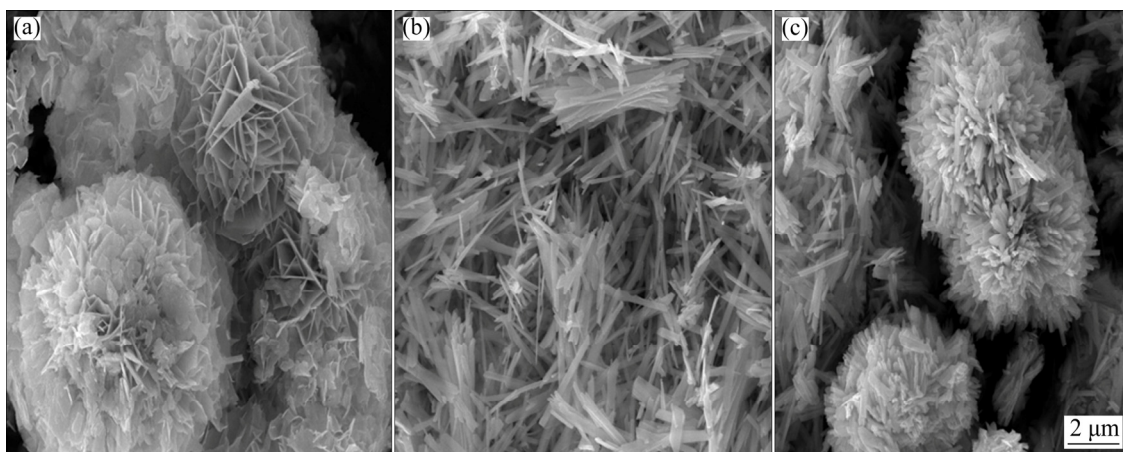


Fig. 3 SEM images of Bi_2S_3 microspheres photocatalysts at different hydrothermal reaction temperatures: (a) 120 °C; (b) 140 °C; (c) 160 °C

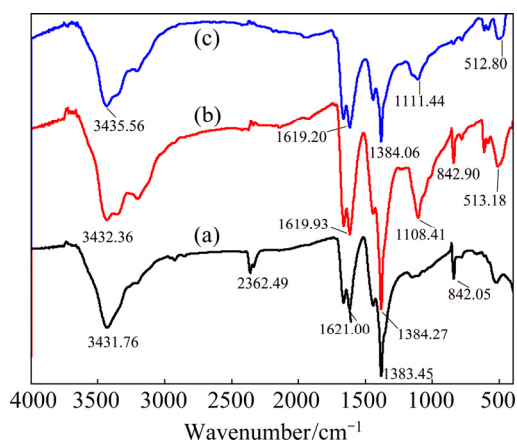


Fig. 4 FT-IR spectra of Bi_2S_3 microspheres photocatalysts with different Bi/S molar ratios: (a) 1:1; (b) 1:2; (c) 1:3

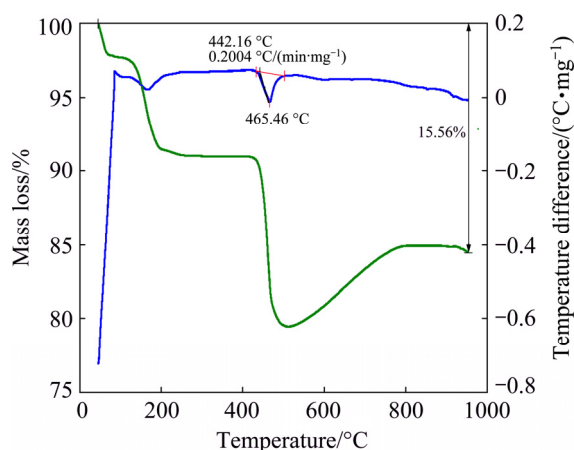


Fig. 5 TG-DTA spectra of Bi_2S_3 microspheres photocatalysts

3.2 Photocatalytic activity of synthetic materials

3.2.1 Effect of Bi/S molar ratio

The effect of the Bi/S molar ratio on the photocatalytic activity of Bi_2S_3 microspheres is shown in Fig. 6. It is obviously observed that the degradation efficiencies of aimed MO dye are 91.07%, 85.48% and 81.64% within 180 min by samples, which were synthesized at different Bi/S molar ratios of 1:1, 1:2 and 1:3, respectively. The blank test shows that the concentration of MO dye keeps stable without Bi_2S_3 microspheres under visible-light irradiation for whole experiment. The experimental results show that the Bi_2S_3 microspheres display the excellent color removal efficiency at the Bi/S molar ratio of 1:1 than the others. The low degradation efficiency at the Bi/S molar ratio of 1:3 may be attributed to the excessive S atoms covering the surface of Bi_2S_3 microspheres and it also can prevent the electron transfer and energy transfer. However, at the Bi/S molar ratio of 1:2, the low photocatalytic activity may be ascribed to a handful of photogenerated electrons captured by Bi_2S_3 microspheres. Hence, the Bi/S molar ratio of 1:1 is the aimed ratio.

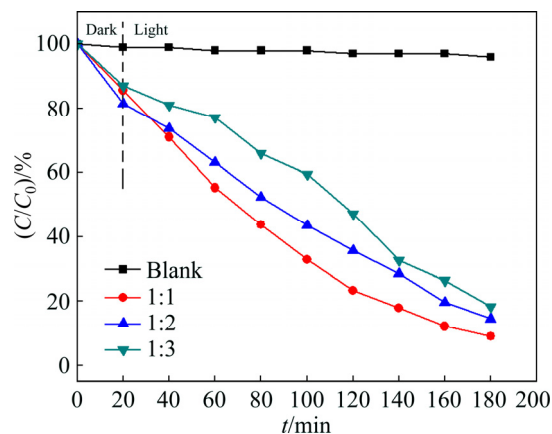


Fig. 6 Effect of Bi/S molar ratio on degradation of MO (15 mg/L) at pH 7.0 under visible light irradiation

3.2.2 Effect of various hydrothermal synthesis reaction temperatures

Figure 7 shows the photodegradation efficiencies of MO for the Bi_2S_3 microspheres at different hydrothermal synthesis reaction temperatures under visible light irradiation. It was obvious that the degradation efficiencies of MO dye by the Bi_2S_3 microspheres are 91.07%, 81.77% and 65.61% at hydrothermal synthesis reaction temperatures of 120, 140 and 160 °C, respectively. Apparently, the hydrothermal synthesis reaction temperature of 120 °C displays the best photocatalytic efficiency under visible light irradiation among the three products. The low photocatalytic activity on the photocatalysts hydrothermal synthesis reaction temperature at 160 °C can be due to the compromised crystallization of Bi_2S_3 microspheres. However, at hydrothermal synthesis reaction temperature of 140 °C, the Bi_2S_3 microsphere has obvious rod structure instead of flower-like structure. This rod structure decreased the surface of samples and contained the electron holes formed.

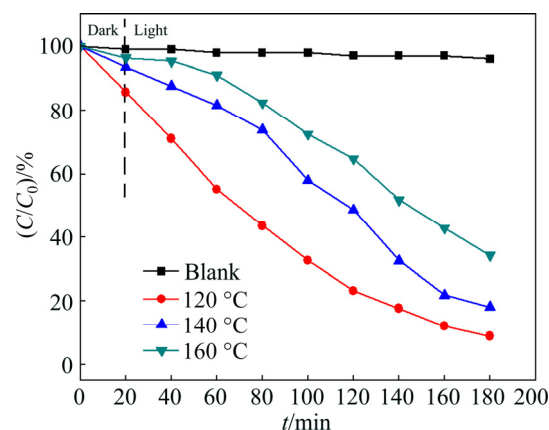


Fig. 7 Effect of hydrothermal synthesis reaction temperature on degradation of MO (15 mg/L) at pH 7.0 under visible light irradiation

3.2.3 Effect of concentration of mineralizer

The effect of mineralizer concentration on the photocatalytic activity of Bi_2S_3 microspheres is depicted in Fig. 8. It can be found that the degradation efficiencies of MO by the catalysts are 63.61%, 91.07% and 84.71% at mineralizer concentrations of 0.8, 1.0 and 1.2 mol/L, respectively. Thus, it can be easily seen that Bi_2S_3 microsphere at mineralizer concentration of 1.0 mol/L presents higher photocatalytic degradation efficiency of MO than the mineralizer concentrations of 0.8 and 1.2 mol/L, due to the different special structures of Bi_2S_3 microsphere. The low photocatalytic activity on the Bi_2S_3 microspheres at mineralizer concentration of 0.8 mol/L, can be ascribed to the small amounts of urea in the process of Bi_2S_3 microspheres synthesis reaction. However, at the mineralizer concentrations of 1.2 mol/L, it can be due to the excessive urea and the small amounts of Bi^{3+} , which led to the bad Bi_2S_3 microspheres crystallization.

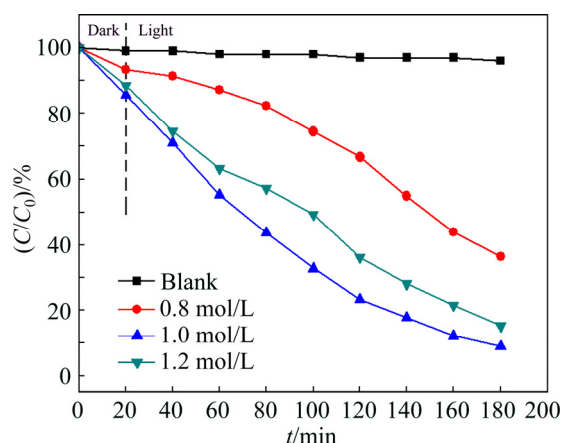


Fig. 8 Effect of mineralizer concentration on degradation of MO (15 mg/L) at pH 7.0 under visible light irradiation

3.2.4 Effect of MO concentration

The photocatalytic activity of Bi_2S_3 microspheres was tested by the degradation of MO under visible-light irradiation at room temperature. Figure 9 shows the effect of MO concentration on the photocatalytic activity of Bi_2S_3 microspheres. Experiments were examined by using the original MO concentration varying from 5 to 25 mg/L at room temperature. It is obviously observed from Fig. 9 that the photodegradation rate of MO increased from 56.10%, 91.07%, to 95.18% with the decrease of the original MO concentrations from 25, 15 to 5 mg/L. It is well known that the Langmuir–Hinshelwood model was used to describe the kinetics of photocatalytic reaction of organic pollutants [30,31]. The reaction kinetic studies suggested that the photocatalytic process of MO follows apparently the pseudo-first-order kinetic equation [32]:

$$\ln \frac{C}{C_0} = k_a t \quad (2)$$

$$t_{1/2} = \frac{\ln 2}{k_a} \quad (3)$$

where k_a stands for the apparent pseudo-first-order rate constant (min^{-1}). Figure 10 indicates the relationships between $\ln(C/C_0)$ and t at different concentrations. All correlated parameters such as k_a , linearization coefficient (R^2) and half-life ($t_{1/2}$) are listed in Table 2. It can be seen from Table 2 that the equations have high regression coefficients (R^2) obviously, which indicates that the photocatalytic reaction is well fitted for the pseudo-first-order kinetic model, especially at different MO concentrations. Furthermore, the products we desired represent the excellent photocatalytic activity at the lowest MO concentration of 5 mg/L. The results may be attributed to the influence of the lowest light transmittance. Besides, amounts of MO molecules will be filled up on the surface of the photocatalyst at the high

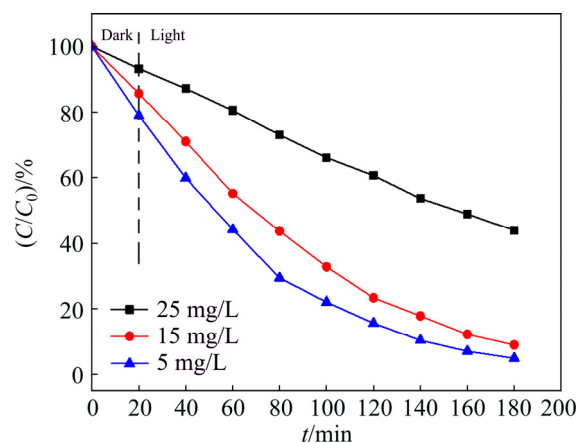


Fig. 9 Effect of original MO concentration on degradation of MO by Bi_2S_3 microspheres photocatalyst at pH 7.0 under visible light irradiation

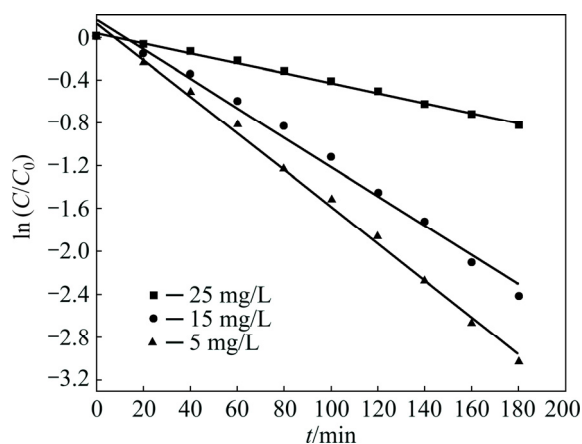


Fig. 10 Relationship between $\ln(C/C_0)$ and t at different original MO concentrations

Table 2 Pseudo-first-order rate constants of photocatalytic degradation

$C_0/$ ($\text{mg}\cdot\text{L}^{-1}$)	Kinetic equation	k_a/min^{-1}	R^2	$t_{1/2}/\text{min}$
5	$Y=-0.01712X$	0.01712	0.99493	40.49
15	$Y=-0.01369X$	0.01369	0.99674	50.63
25	$Y=-0.00464X$	0.00464	0.99363	149.39

initial MO concentration, which hinders the adsorption of light on the surface of the photocatalyst. Desiring the high photodegradation rate and efficient use of light, the MO concentration of 15 mg/L is the optimized original concentration.

In order to authenticate the photocatalytic activity of Bi_2S_3 microsphere, the effectiveness of the Bi_2S_3 microsphere was compared with other photocatalyst. As found in Table 3, it is clear that the Bi_2S_3 microsphere shows higher visible photocatalytic activity than the other photocatalysts. So, the aimed synthesis of Bi_2S_3 microsphere is desirable considering the low-cost, convenient fabrication and visible-light-driven.

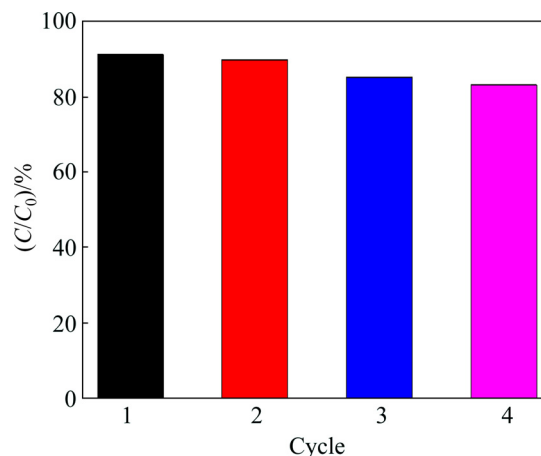
Table 3 Photocatalytic activity of photocatalysts for MO

Photocatalytic	Light source	Result	Ref.
ZnO	UV-light	Removal rate was about 89% in 240 min	[33]
$\text{Bi}_4\text{TaO}_8\text{I}$	Solar light	Removal rate was about 89% in 600 min	[34]
$\text{NaTaO}_{3-x}\text{N}_x$	Sunlight	Removal rate was about 100% in 840 min	[35]
$\text{Bi}_2\text{O}_3/\text{g}-\text{C}_3\text{N}_4$	UV-light	Removal rate was about 90% in 360 min	[36]
TiO_2	Solar light	Removal rate was about 60 % in 360 min	[37]

3.2.5 Stability and reusability

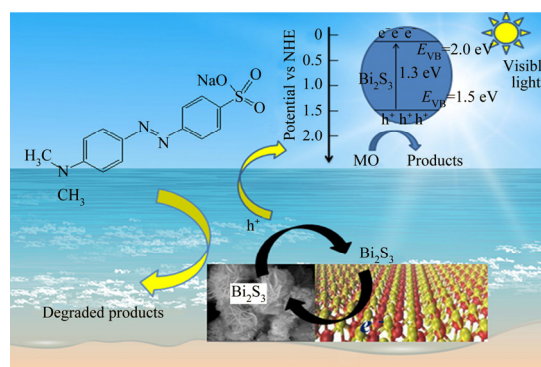
It is an important factor to study the regeneration of the samples in the selection of a catalyst for photocatalytic degradation of organic pollutants. In order to obtain the stability and reusability of the products, the repeated photodegradation of MO by Bi_2S_3 microsphere was inspected. After four respective cycles, the catalyst still keeps relatively continual photocatalytic performance under visible light irradiation. The results are shown in Fig. 11. The renewable photocatalysts were recovered by centrifugation, washed successively with distilled water and anhydrous ethanol, and then dried in the vacuum oven at 60 °C overnight. From Fig. 11, it can be easily found that the catalyst efficiency of Bi_2S_3 microsphere can still remain higher than 80% after the Bi_2S_3 microsphere reused three times. Based on the

above explanation, this Bi_2S_3 microsphere could be used as an efficient and promising photocatalyst.

**Fig. 11** Photocatalytic cycles of Bi_2S_3 samples at pH 7.0 under visible light irradiation

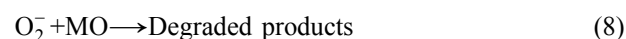
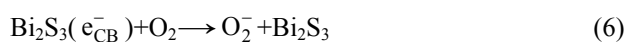
3.2.6 Photodegradation mechanism of Bi_2S_3 microsphere

On the basis of the above mentioned Bi_2S_3 microsphere, the light absorption by the samples and the separation of the photoelectrons and holes are the significant factors in the process of the photocatalytic reaction, the tentatively photodegradation mechanism of Bi_2S_3 microsphere is illustrated in Fig. 12. Bi_2S_3 microsphere can absorb visible light by virtue of the narrow band gap of 1.3 eV.

**Fig. 12** Possible schemes for electron-hole separation and transport at Bi_2S_3 microsphere photocatalyst interface

Under the visible irradiation, Bi_2S_3 microsphere can be easily inspired to yield photon-generated carries. And produced electrons from the valence band are then easily transferred to the appropriate power conduction band, leaving lots of holes in the valence band of Bi_2S_3 microsphere. Better yet, the special structure of samples can availably restrain the recombination of photoelectrons and holes so that the photocatalytic activity is improved. The holes located in the valence band of photocatalyst can promote the formation of hydroxyl radicals ($\cdot\text{OH}$) from OH groups absorbed on

the surface [38,39]. Besides, the electrons are eliminated by the absorbed molecular oxygen (O_2) to form O_2^- radicals. The radical ions $\cdot OH$ and O_2^- will cause the decomposition of MO. The major reaction steps for photodegradation of MO under visible-light irradiation may be proposed as Eqs. (4)–(8).



4 Conclusions

1) The Bi_2S_3 microsphere was successfully synthesized by one-pot hydrothermal methods. Besides, the mineralizer of urea introduced can effectively restrain the recombination of photoelectrons and holes and improve the photocatalytic activity.

2) At the optimum of Bi/S molar ratio of 1:1, hydrothermal synthesis reaction temperature of 120 °C, concentration of mineralizer of 1.0 mol/L and initial MO concentration of 15 mg/L, the prepared samples have an excellent photocatalytic activity (91.07%) for degradation of MO under visible-light irradiation.

3) The Bi_2S_3 microsphere represents a good stability and reusability for the degradation ratio of MO still keeps higher than 80% after three cycles.

4) The Bi_2S_3 microsphere as a stable, simple synthesis and low cost raw material with outstanding photocatalytic activity can be applied as high-efficiency photocatalyst for the dye degradation in waste water treatment. Meanwhile, the mechanism and preparation method reported could be easily transferred to prepare other materials for different applications.

References

- [1] HASSANZADEH-TABRIZI S A, MOTLAGH M M, SALAHSHOUR S. Synthesis of ZnO/CuO nanocomposite immobilized on γ - Al_2O_3 and application for removal of methyl orange [J]. *Applied Surface Science*, 2016, 384: 237–243.
- [2] ZHOU Y M H, SHUAI L, JIANGI X Y, JIAO F P, YU J G. Visible-light-driven photocatalytic properties of layered double hydroxide supported Bi_2O_3 modified by Pb(II) for methylene blue [J]. *Advance Power Technology*, 2015, 26: 439–447.
- [3] WANG A L, CHEN L, ZHANG J X, SUN W C, GUO P, REN C Y. Ionic liquid microemulsion-assisted synthesis and improved photocatalytic activity of $ZnIn_2S_4$ [J]. *Journal of Materials Science*, 2017, 52: 2413–2421.
- [4] MOTLAGH M M, HASSANZADEH-TABRIZI S A, SAFFAR-TELURI A. Sol-gel synthesis of $Mn_2O_3/Al_2O_3/SiO_2$ hybrid nanocomposite and application for removal of organic dye [J]. *Journal of Sol-Gel Science Technology*, 2015, 73: 9–13.
- [5] LI X Y, LI X, WANG J, ZHAI H J, CHEN X B. Synthesis of ZnSe microdisks and nanobelts and their visible-light photocatalytic properties [J]. *Journal of Materials Science*, 2017, 52: 3821–3830.
- [6] SCHLICHTER S, DIEZ A S, ZENOBI M C, DENNEHY M, ALVAREZI M. Multi-metal-substituted-goethite as an effective catalyst for azo dye [J]. *Clean-Soil, Air, Water*, 2016, 44: 1652–1660.
- [7] LI X P, CHEN Y B, HU X Y, ZHANG Y F, HU L J. Desalination of dye solution utilizing PVA/INDF hollow fiber composite membrane modified with TiO_2 nanoparticles [J]. *Journal of Membrane Science*, 2014, 471: 118–129.
- [8] KHAN S A, KHAN S B, ASIRI A M. Toward the design of Zn–Al and Zn–Cr LDH wrapped in activated carbon for the solar assisted de-coloration of organic dyes [J]. *RSC Advance*, 2016, 6: 83196–83208.
- [9] LE S K, JIANG T S, LI Y W, ZHAO Q, LI Y Y, FANG W B, GONG M. Highly efficient visible-light-driven mesoporous graphitic carbon nitride/ZnO nanocomposite photocatalysts [J]. *Applied Catalysis B: Environmental*, 2017, 200: 601–610.
- [10] BAO H F, LI C M, CUI X Q, GAN Y, SONG Q L, GUO J. Synthesis of a highly ordered single-crystalline Bi_2S_3 nanowire array and its metal/semiconductor/metal back-to-back Schottky [J]. *Small*, 2008, 4: 1125–1129.
- [11] LI D B, HU L, XIE Y, NIU G D, LIU T F, ZHOU Y H, GAO L, YANG B, TANG J. Low-temperature-processed amorphous Bi_2S_3 film as an inorganic electron transport layer for perovskite solar cells [J]. *ACS Photonics*, 2016, 3: 2122–2128.
- [12] SUN B, DONG J, SHI W J, AI S Y. A hierarchical charge transport cascade based on W- Bi_2S_3 /poly(thiophenyl-3-boronic acid) hybrid for robust photoelectrochemical analysis of subgroup J of avian leukosis virus [J]. *Sensors and Actuators B: Chemical*, 2016, 229: 75–81.
- [13] NIE G D, LU X F, LEI J Y, YANG L, WANG C. Facile and controlled synthesis of bismuth sulfide nanorods-reduced graphene oxide composites with enhanced supercapacitor performance [J]. *Electrochimica Acta*, 2015, 154: 24–30.
- [14] GUO D L, HU C G, ZHANG C L. First-principles study on doping and temperature dependence of thermoelectric property of Bi_2S_3 thermoelectric material [J]. *Materials Research Bulletin*, 2013, 48: 1984–1988.
- [15] JIARUI J, TAO H. Facile synthesis of Bi_2S_3 nanoribbons for photocatalytic reduction of CO_2 into CH_3OH [J]. *Applied Surface Science*, 2017, 394: 364–370.
- [16] WU T, ZHOU X G, ZHANG H, ZHONG X H. Bi_2S_3 nanostructures: A new photocatalyst [J]. *Nano Research*, 2010, 3: 379–386.
- [17] PRABHAKAR VATTIKUTI S V, BAIK Y J, BYON C. Enhanced photocatalytic activity of MoO_3 -supported SnO_2 composite synthesized by a wet chemical method [J]. *Materials Express*, 2016, 6(2): 161–174.
- [18] PRABHAKAR VATTIKUTI S V, BYON C. Bi_2S_3 nanorods embedded with MoS_2 nanosheets composite for photodegradation of phenol red under visible light irradiation [J]. *Superlattices and Microstructures*, 2016, 100: 514–525.
- [19] HU E, GAO X, ETOGO A, XIE Y, ZHONG Y, HU Y. Controllable one-pot synthesis of various one-dimensional Bi_2S_3 nanostructures and their enhanced visible-light-driven photocatalytic reduction of Cr(VI) [J]. *Journal of Alloys and Compounds*, 2014, 611: 335–340.
- [20] PRABHAKAR VATTIKUTI S V, SHIM J, BYON C. Synthesis, characterization, and optical properties of visible light-driven Bi_2S_3 nanorod photocatalysts [J]. *Journal of Materials Science—Materials in Electronics*, 2017, 28(19): 14282–14292.
- [21] ZHANG D, ZHAO G Q, YU J G, JIAO F P, YAN T, ZHU M Y. Thermodynamic and kinetic studies of effective adsorption of 2,4,6-trichlorophenol onto calcine Mg/Al- CO_3 layered double

- hydroxide [J]. Journal of Wuhan University of Technology, 2016, 31: 1211–1218.
- [22] WANG F, WANG Z J, ZHU J F, YANG H B, CHEN X J, WANG L, YANG C H. Facile synthesis SnO₂ nanoparticle-modified Ti₃C₂ MXene nanocomposites for enhanced lithium storage application [J]. Journal of Materials Science, 2017, 52: 3556–3565.
- [23] ZHAO G Q, LI C F, WU X, YU J G, JIANG X Y, HU W J H, JIAO F P. Reduced graphene oxide modified NiFe-calcinated layered double hydroxides for enhanced photocatalytic removal methylene blue [J]. Applied Surface Science, 2018, 434: 251–259.
- [24] ZHU Z, LU Z Y, WANG D D, TANG X, YAN Y S, SHI W D, WANG Y S, GAO N L, YAO X, DONG H J. Construction of high-dispersed Ag/Fe₃O₄/g-C₃N₄ photocatalyst by selective photo-deposition and improved photocatalytic activity [J]. Applied Catalysis B: Environmental, 2016, 182: 115–122.
- [25] RONG J, ZHANG T, QIU F X, RONG X S, ZHU X L, ZHANG X Y. Preparation of hierarchical micro/nanostructured Bi₂S₃-WO₃ composites for enhanced photocatalytic performance [J]. Journal of Alloys and Compounds, 2016, 685: 812–819.
- [26] OTA J, SRIVASTAVA S K. Polypyrrole coating of tartaric acid-assisted synthesized Bi₂S₃ nanorods [J]. The Journal of Physical Chemistry C, 2007, 111: 12260–12264.
- [27] KE J, LIU J, SUN H Q, ZHANG H Y, DUAN X G, LIANG P, LI X Y, TADE M O, LIU S M, WANG S B. Facile assembly of Bi₂O₃/Bi₂S₃/MoS₂ n-p heterojunction with layered n-Bi₂O₃ and p-MoS₂ for enhanced photocatalytic water oxidation and pollutant degradation [J]. Applied Catalysis B—Environmental, 2017, 200: 47–55.
- [28] GAO T T, YU J G, ZHOU Y, JIANG X Y. The synthesis of graphene oxide functionalized with dithiocarbamate group and its prominent performance on adsorption of lead ions [J]. Journal of The Taiwan Institute of Chemical Engineers, 2017, 71: 426–432.
- [29] KUN W N, MLOWE S, NYAMEN L D, NDIKON P T, MALIK M A, MUNRO O Q, REVAPRASADU N. Heterocyclic bismuth (III) dithiocarbamate complexes as single-source precursors for the synthesis of anisotropic Bi₂S₃ nanoparticles [J]. Chemistry: A European Journal, 2016, 22: 13127–13135.
- [30] YU J G, ZHOU M H, YU H G, ZHANG Q J, YU Y. Enhanced photoinduced super-hydrophilicity of the sol-gel-derived TiO₂ thin films by Fe-doping [J]. Materials Chemistry and Physics, 2006, 95: 193–196.
- [31] ZHAO Y X, TENG F, XU J, LIU Z L, YANG Y, ZHANG Q Q, YAO W Q. Facile synthesis of Cu₂PO₄OH hierarchical nanostructures and their improved catalytic activity by a hydroxyl group [J]. RSC Advance, 2015, 5: 100934–100942.
- [32] WU X, ZHANG D, JIAO F P, WANG S. Visible-light-driven photodegradation of methyl orange using Cu₂O/ZnAl calcined layered double hydroxides as photocatalysts [J]. Colloids and Surfaces A, 2016, 508: 110–116.
- [33] KANSAL S K, SINGH M, SUD D. Studies on photodegradation of two commercial dyes in aqueous phase using different photocatalysts [J]. Journal of Hazardous Materials, 2007, 141: 581–590.
- [34] FAN J, HU X, XIE Z, ZHANG K, WANG J. Photocatalytic degradation of azo dye by novel Bi-based photocatalyst Bi₄TaO₈I under visible-light irradiation [J]. Chemical Engineering Journal, 2012, 179: 44–51.
- [35] LIU D R, JIANG Y S, GAO G M. Photocatalytic degradation of an azo dye using N-doped NaTaO₃ synthesized by one-step hydrothermal process [J]. Chemosphere, 2011, 83: 1546–1552.
- [36] LI Y P, WU S L, HUANG L Y, XU H, ZHANG R X, QU M L, GAO Q, LI H M. g-C₃N₄ modified Bi₂O₃ composites with enhanced visible-light photocatalytic activity [J]. Journal of Physics and Chemistry of Solids, 2015, 76: 112–119.
- [37] ONG S A, MIN O M, HO L N, WONG Y S. Solar photocatalytic degradation of mono azo methyl orange and diazo reactive green 19 in single and binary dye solution: Adsorbability vs photodegradation rate [J]. Environmental Science and Pollution Research, 2013, 20: 3405–3413.
- [38] ZHU C S, ZHENG J T, FANG L Y, HU P, LIU Y K, CAO X Q, WU M B. Advanced visible-light driven photocatalyst with enhanced charge separation fabricated by facile deposition of Ag₃PO₄ nanoparticles on graphene-like h-BN nanosheets [J]. Journal of Molecular Catalysis A: Chemical, 2016, 424: 135–144.
- [39] MA J, DING J, YU L, LI L, KONG Y, KOMARNENI S. BiOCl dispersed on NiFe-LDH leads to enhanced photo-degradation of Rhodamine-B dye [J]. Applied Clay Science, 2015, 109: 76–82.

硫化铋微球的制备及其可见光下高效光催化性能

赵国庆^{1,2}, 郑怡健¹, 贺治国³, 卢泽湘⁴, 王龙¹, 李彩凤¹, 焦飞鹏^{1,2}, 邓春燕¹

1. 中南大学 化学化工学院, 长沙 410083;

2. 中南大学 锰资源高效清洁利用湖南省重点实验室, 长沙 410083;

3. 中南大学 资源加工与生物工程学院, 长沙 410083;

4. 福建农林大学 材料工程学院 化学工程系, 福州 350002

摘要: 通过一步尿素辅助水热法合成新颖的硫化铋微球, 对合成的硫化铋微球采用 X 射线衍射(XRD)、扫描电镜(SEM)、红外光谱(FT-IR)和差示扫描量热法和热重分析法(DTA-TG)进行表征。随后, 在可见光照射条件下, 通过光降解甲基橙模拟溶液对硫化铋微球的光催化活性进行评估。实验结果表明, 在 180 min 内, 硫化铋微球光降解效率可达 91.07%, 且其可作为一种潜在高效的催化剂用于溶液中甲基橙的去除。同时, 依据催化剂价带位置提出了可能性的光降解机理途径。因此, 本实验设计了一种可见光响应的光催化剂, 并可作为一种有效的光催化剂用于太阳能转换和环境污染处理领域。

关键词: 硫化铋微球; 水热法; 光催化降解